Advances in Science and Technology Research Journal

Advances in Science and Technology Research Journal, 2026, 20(2), 504–514
https://doi.org/10.12913/22998624/213730
ISSN 2299-8624, License CC-BY 4.0

Received: 2025.08.02
Accepted: 2025.12.15
Published: 2025.12.23

The effect of viscous damping on dynamic response of flexure-based mechanisms

Huy-Hoang Pham[1], Quoc-Nhiem Tran[1], Van-Khien Nguyen[1*]

[1] Ho Chi Minh City University of Industry and Trade, Ho Chi Minh City, Vietnam
* Corresponding author's e-mail: khiennv@huit.edu.vn

ABSTRACT

This paper presents an intriguing study on the influence of damping oil to the transient response of the displacement output of a flexure-based mechanism when comparing the responses in two cases working in or not in lubrication oil. The mechanism includes two flexure amplifier levers connected by a bar with two flexure hinges creating a structure of flexure four bar linkage. Prior to fabrication, the designed flexure mechanism was evaluated with two models: numerical Ansys model and pseudo rigid body model with Matlab Simulink. The models were used to predict transient response in terms of displacement and stress under viscous damping. Then the results of modeling and simulation were validated by experiments. Both numerical simulations and experimental results show that the output displacement responses including overshoot and response time are significantly reduced when the applying viscous damping of lubrication oil. Specifically, experiments showed that overshoot and response time were (0.272 mm, 0.05 s) when counting viscous damping, in comparison with (0.341 mm, 0.1 s) when not. These findings open a new study-direction in the application of flexure-based mechanisms in different working environments.

Keywords: flexure mechanism, pseudo rigid-body diagram, damping, dynamic response.

INTRONDUCTION

Flexure mechanism has no backlash, no dry friction, no need of lubrication and high stiffness. Therefore, flexure mechanisms can provide precision small motion with high resolution. Flexure-based mechanisms are increasingly used in various fields such as precision fabrication systems [1, 2], accurate displacement generation and precise positioning [3], medical assisting systems [4], precise grippers [5], force stabilization [6], and force stabilization systems of robot arms and end-effector [7, 8]. Their applications extend to fluid control [9, 10] and even aerospace engineering thanks to their advantages: compactness, easy integration, smooth motion, frictionless operation, no need of lubrication and high stiffness and precision [11, 12]. Recent studies have focused on developing new large displacement amplification and high natural frequencies while maintaining material strength for high-performance operation. Intelligent control algorithms have also been created to improve control accuracy and minimize errors [13]. To receive the optimal design on the shape and dimensions of flexure mechanisms, finite element analysis (FEA) commercial software like Ansys, Abacus, etc. [14], or topology optimization [15, 16], and mathematical modeling [17] are employed [14]. Recently, some studies have incorporated damping coefficients at the flexure joints into the modeling and analysis [18, 19]. Other works combine flexure-based mechanisms with pneumatic pressure control to compensate the errors for manufacturing and positioning errors of piezo (PZT) actuators [20]. However, most previous studies involved modeling, simulation and experiments with flexure mechanisms

in environment without counting the viscous damping with temperature between 20–28 °C. Actually, in real-world applications, these mechanisms can work in various environments such as water, lubrication oil, or gas. Oil provides viscous damping that reduces overshoot and oscillation, and minimizes settling time. Therefore, flexure stages in scanning probes of microscopes can be immersed in damping fluid for faster stabilization. In addition, immersing flexure structures of precision instruments in oil reduces wear, prevents corrosion, and ensures long-term reliability. Compliant suspensions of gyroscopes or inertial sensors can be immersed into oil for stability. Another application can be seen when damping of flexures in oil-immersion microscope objectives reduces drift thanks to oil immersion of optical and imaging systems reduces vibrations and provides a stable refractive index medium. Therefore, studying how flexure mechanisms work in different environments is essential. This study proposes a new approach: dynamic response of a flexure-based mechanism working with an open-loop control system and dipped to lubrication oil. The performance is compared in both cases dipped to oil and left in the air to evaluate the oil's viscous damping on dynamic response characteristics. The flexure mechanism involved to the proposed study uses semi-circular elastic flexure hinges combined with rigid bars. Firstly, the mechanism is mathematically modeled to consider the viscosity and viscous friction while it is immersed in oil. The mathematical model and numerical model are respectively simulated using Matlab Simulink and Ansys to determine the displacement, stress and dynamic responses such as the overshoot and the response time. Finally, the mechanism was fabricated using wire-cutting CNC, armed with PZT actuator and displacement sensor and used for experimentation.

PROBLEM FORMULATION

Operational principle

The flexure mechanism is designed using two amplifier levers (Figure 1). The output of shorter lever is transferred to the longer lever as its input thanks to a connection bar. All revolute joints are semi-circular flexure joints. The whole mechanism is a monolithic structure flexure four bar linkage. It is driven by a PZT actuator. The

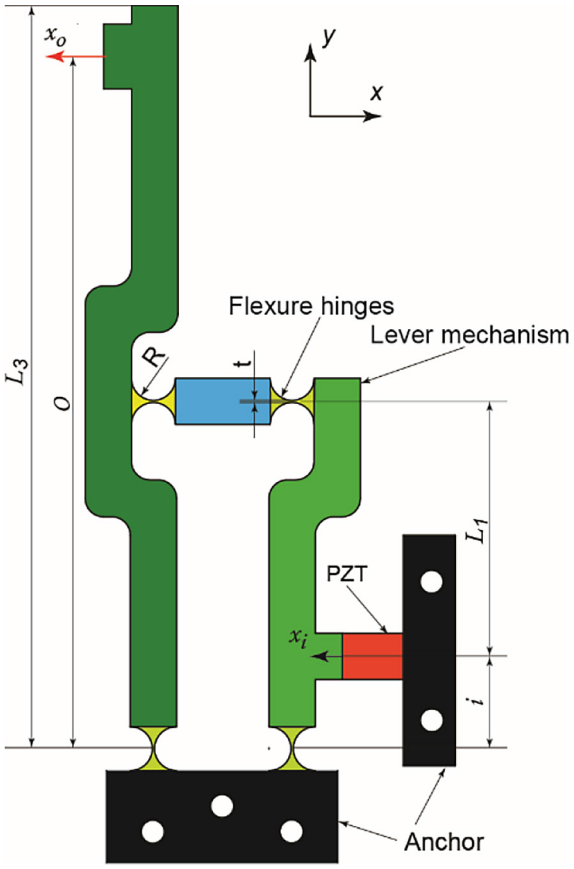

Figure 1. Schematic diagram of the linear flexure-based mechanism

generated input displacement x_i by PZT actuator is amplified by two levers and produces the desired output displacement x_o.

Dynamic analysis of flexure mechanism dipped to lubrication oil

The pseudo-rigid-body model is illustrated in Figure 2, where (i = 1, 2, 3), represent mass, length, moment of inertia, and damping coefficients of the rigid links, respectively. The linear stiffness and torsional stiffnesses of semi-circular flexure joints can be determined by Equations (1) and (2) [21]. Figure 3 shows the input and output displacements (x_i, x_o) là x_i and x_o, and coordinates (s_1, s_3) of center-of-mass S_i.

$$\textit{Linear stiffness } k \text{ (N/m)}: \frac{1}{k} = \\ = \frac{1}{Eb}\left[\pi\left(\frac{R}{t}\right)^{1/2} - 2.57\right] \quad (1)$$

$$\textit{Torsional stiffness } k_\theta \text{ (Nm/rad)}: \frac{1}{k_\theta} = \frac{9\pi R^{1/2}}{2Ebt^{5/2}} \quad (2)$$

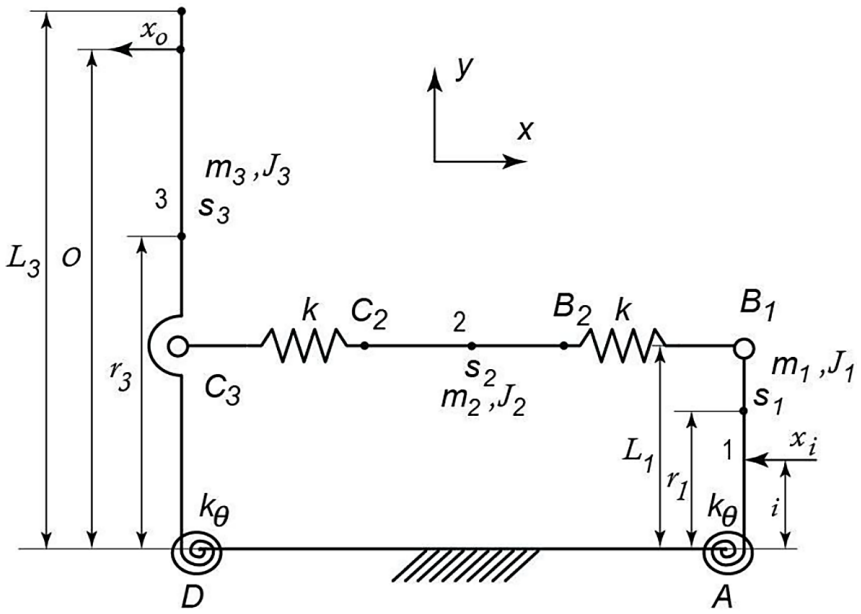

Figure 2. The pseudo-rigid-body model diagram

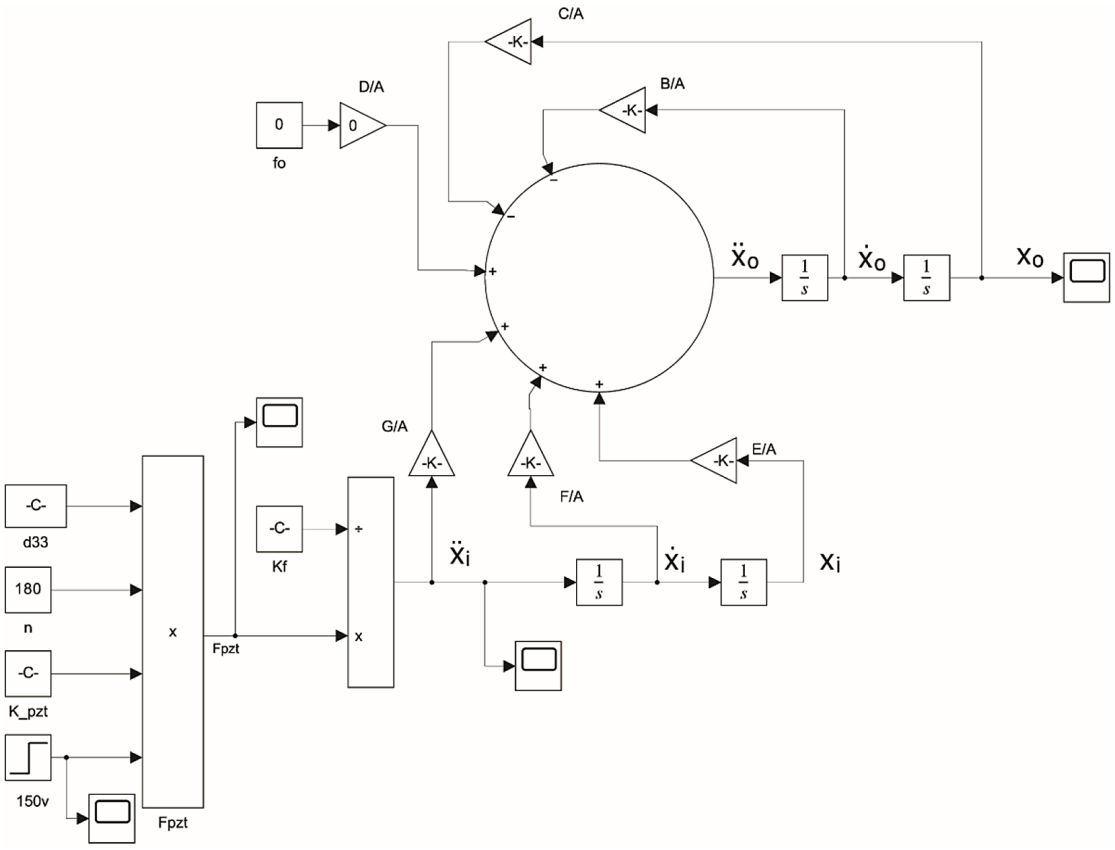

Figure 3. Matlab Simulink model

where: E, b_i, T_i, R_i are the Young's modulus of the material (200 GPa corresponding to carbon steel C45), the out-of-plane thickness, the minimum width, and the radius of the hinges, respectively.

From the numerical model built in Solidwork, we have the surface areas of one side, weights and coordinates of centers of mass:

- $A_1 = 3.75 \cdot 10^{-3}$ m^2; $m_1 = 0.075$ kg; $s_1 = 0.05$ m;
- $A_2 = 1.03 \cdot 10^{-3}$ m^2; $m_2 = 0.021$ kg;

- $A_3 = 7.36 \cdot 10^{-3}$ m^2; $m_3 = 0.15$ kg; $s_3 = 0.093$ m;

The viscous damping of lubrication oil is produced by viscous friction (a form of wet friction) which is proportional to the relative velocity. The constant of proportionality is the damping coefficient determined in Equation 3. The lubrication oil has technical characteristics: Specific gravity $\rho = 850$ kg/m^3, kinematic viscosity: $\mu = 95.9$ cSt and dynamic viscosity: $\eta = 81.52 \cdot 10^{-3}$ Ns/m^2; The damping coefficient (viscous damping ratio) can be estimated from the oil viscosity, surface area of fluid contact and the distance of velocity gradient:

$$c = \eta A / d \tag{3}$$

where: η is the dynamic viscosity of the fluid (oil); A is the surface area of the plate in contact with the fluid – it is calculated as the double of surface area of one side A_i (i = 1, 2, 3) because two sides of the mechanism contact oil; d is the thickness of the fluid layer affected by the motion (often related to the boundary layer thickness), here d = 0.002 m.

Therefore, $c_1 = 0.305$ Ns/m; $c_2 = 0.084$ Ns/m and $c_3 = 0.6$ Ns/m. The kinematic parameters including lever rotation angles φ_i, rotation velocities φ_1 and velocities of center of mass v_{s1} of the mechanism are shown as follows:

$$\begin{aligned} &\varphi_1 = \frac{x_i}{i} = \frac{x_{S_1}}{s_1};\ \dot{\varphi}_1 = \frac{\dot{x}_i}{i};\ v_{S_1} = \dot{x}_{S_1} = \frac{s_1}{i}\dot{x}_i \\ &\varphi_3 = \frac{x_o}{o} = \frac{x_{S_3}}{s_3};\ \dot{\varphi}_3 = \frac{\dot{x}_o}{o};\ v_{S_3} = \dot{x}_{S_3} = \frac{s_3}{o}\dot{x}_o \\ &v_{S_2} = \dot{x}_2 \end{aligned} \tag{4}$$

The input point is supposed pushed gradually therefore $f_i = 0$; The load at output is f_o; the kinematic energy of the mechanism is

$$\begin{aligned} E_k = \frac{1}{2}m_1\left(\frac{s_1}{i}\right)^2\dot{x}_i^2 + \frac{1}{2}j_1\frac{\dot{x}_i^2}{i^2} + \\ + \frac{1}{2}m_3\left(\frac{s_3}{o}\right)^2\dot{x}_o^2 + \frac{1}{2}j_3\frac{\dot{x}_o^2}{o^2} + \frac{1}{2}m_2\dot{x}_2^2 \end{aligned} \tag{5}$$

The potential energy of the mechanism is

$$\begin{aligned} E_p = \frac{1}{2}k_\theta\left(\frac{x_i}{i}\right)^2 + \frac{1}{2}k_\theta\left(\frac{x_o}{o}\right)^2 + \\ + \frac{1}{2}k\left(x_2 - l_1\frac{x_i}{i}\right)^2 + \frac{1}{2}k\left(x_2 - l_1\frac{x_o}{o}\right)^2 \end{aligned} \tag{6}$$

The power of external load is

$$P = -f_o \cdot \dot{x}_o \tag{7}$$

The energy dissipation function is

$$\Delta = \Delta_1 + \Delta_2 + \Delta_3 \tag{8}$$

where: velocity changes along the length of the lever therefore the energy dissipation function of the shorter lever is

$$\Delta_1 = \int_0^{l_1}\left[\frac{1}{2}c_1^y(y\dot{\varphi}_1)^2\right]dy = \frac{1}{6}c_1\left(\frac{l_1}{i}\right)^2\dot{x}_i^2 \tag{9}$$

The connection bar horizontally translates therefore the energy dissipation function of connection bar is

$$\Delta_2 = \frac{1}{2}c_2\dot{x}_2^2 \tag{10}$$

Velocity changes along the length of the lever therefore the energy dissipation function of longer lever is

$$\Delta_3 = \int_0^{l_3}\left[\frac{1}{2}c_3^y(y\dot{\varphi}_3)^2\right]dy = \frac{1}{6}c_3\left(\frac{l_3}{o}\right)^2\dot{x}_o^2\ 8 \tag{11}$$

Apply the above functions Equation 5–11 to the Lagrange's equation Equation 12 we have the results in equation system Equation 13, 14, 15:

$$\frac{d}{dt}\left(\frac{\partial E_k}{\partial \dot{q}_i}\right) + \frac{\partial E_p}{\partial q_i} = \frac{\partial(P - \Delta)}{\partial \dot{q}_i} \tag{12}$$

Where q_i is one of general coordinates of the system $\{x_i, x_2, x_o\}$.

$$\begin{aligned} \left[m_1\left(\frac{s_1}{i}\right)^2 + \frac{j_1}{i^2}\right]\ddot{x}_i + \left[k\left(\frac{l_1}{i}\right)^2 + \frac{k_\theta}{i^2}\right]x_i - \\ -k\frac{l_1}{i}x_2 = -\frac{1}{3}c_1\left(\frac{l_1}{i}\right)^2\dot{x}_i \end{aligned} \tag{13}$$

$$\begin{aligned} \left[m_3\left(\frac{s_3}{o}\right)^2 + \frac{j_3}{o^2}\right]\ddot{x}_o + \left[k\left(\frac{l_1}{o}\right)^2 + \frac{k_\theta}{o^2}\right]x_o - \\ - k\frac{l_1}{o}x_2 = -f_o - \frac{1}{3}c_3\left(\frac{l_3}{o}\right)^2\dot{x}_o \end{aligned} \tag{14}$$

$$m_2\ddot{x}_2 + 2kx_2 - k\frac{l_1}{i}x_2 - k\frac{l_1}{o}x_o = -c_2\dot{x}_2 \tag{15}$$

The dynamic response of output x_o to the input x_i and load f_o is derived using equation system (13, 14, 15):

$$\begin{aligned} \left[m_3\left(\frac{s_3}{o}\right)^2 + \frac{j_3}{o^2}\right]\ddot{x}_o + \frac{1}{3}c_3\left(\frac{l_3}{o}\right)^2\dot{x}_o + \\ + \left[k\left(\frac{l_1}{o}\right)^2 + \frac{k_\theta}{o^2}\right]x_o = -f_o + \\ + \frac{i}{o}\left\{\begin{array}{c}\left[m_1\left(\frac{s_1}{i}\right)^2 + \frac{j_1}{i^2}\right]\ddot{x}_i + \\ + \frac{1}{3}c_1\left(\frac{l_1}{i}\right)^2\dot{x}_i + \left[k\left(\frac{l_1}{i}\right)^2 + \frac{k_\theta}{i^2}\right]x_i\end{array}\right\} \end{aligned} \tag{16}$$

Organize the parameters as belows

$$A = \left[m_3\left(\frac{s_3}{o}\right)^2 + \frac{j_3}{o^2}\right];$$
$$B = \frac{1}{3}c_3\left(\frac{l_3}{o}\right)^2; C = \left[k\left(\frac{l_1}{o}\right)^2 + \frac{k_\theta}{o^2}\right];$$
$$D = -f_o; E = \frac{i}{o}\left[m_1\left(\frac{s_1}{i}\right)^2 + \frac{j_1}{i^2}\right]; \quad (17)$$
$$F = \frac{1}{3}\frac{i}{o}c_1\left(\frac{l_1}{i}\right)^2; G = \frac{i}{o}\left[k\left(\frac{l_1}{i}\right)^2 + \frac{k_\theta}{i^2}\right]$$

where: the dimensions are: i = 0.02 m; o = 0.15 m; s_1 = 0.048 m; s_3 = 0.093 m; l_1 = 0.075 m; l_3 = 0.163 m.

We have the dynamic response of output x_o to the input x_i described as

$$A\ddot{x}_o + B\dot{x}_o + Cx_o = \\ = D + E\ddot{x}_i + F\dot{x}_i + Gx_i \quad (18)$$

The dynamic response of output x_o to the input x_i is performed using Matlab Simulink as follows. The Matlab Simulink model (Figure 3) is built based on the mathematical model in Equation 18.

Table 1. Matlab Simulink simulation parameters

Design variables	Value	Design variables	Value
i	0.02 m	t	0.5e-3 m
o	0.15 m	b	10e-3 m
S_1	0.048 m	R	9.5e-3 m
S_3	0.093 m	C_1	0.305 Ns/m
L_1	0.075 m	C_2	0.084 Ns/m
L_3	0.163 m	C_3	0.6 Ns/m

The modeling parameters can be seen in Table 1. The Matlab Simulink model is used to simulate the dynamic response of the flexure mechanism in two cases: the mechanism is immersed to lubrication oil (nonzero damping coefficients) or is left in the air (zero damping coefficients). The transient response simulation is shown in Figures 4 and 5. The results indicate improved performance in the presence of damping oil, with a response time of 0.184 s, better than 0.286 s when without oil damping.

Transient response simulation using Ansys

The design was numerically constructed as a 3D Inventor model and then transferred to Ansys Workbench for performing finite element analysis to simulate the displacement and stress behaviors of the flexure mechanism. The 3D model is meshed using 88,470 3D Solid186 elements and specified to material carbon steel C45 (E = 200 GPa, Poisson's ratio = 0.3, yield strength = 250 MPa, density = 7850 kg/m³).

The damping constant of the oil is set to the Ansys model and specified in the in Analysis Settings – Damping Controls – Constant Structural Damping Coefficient. The meshing of the mechanism can be seen in Figure 6 with Solid186 Tetrahedral elements. We use the Transient structural module of Ansys to perform the transient analysis and simulation. The boundary conditions are

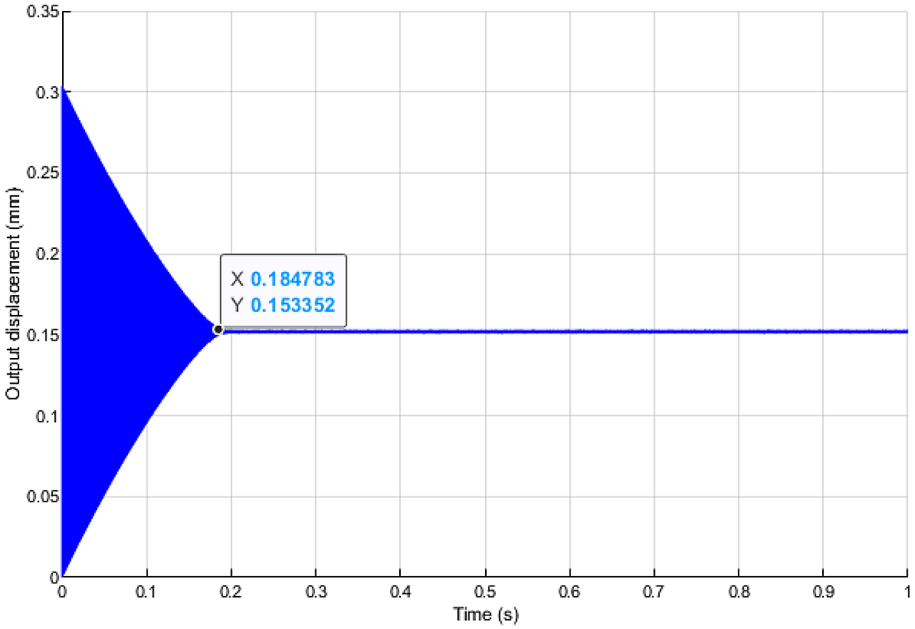

Figure 4. Matlab Simulink simulations (with oil damping)

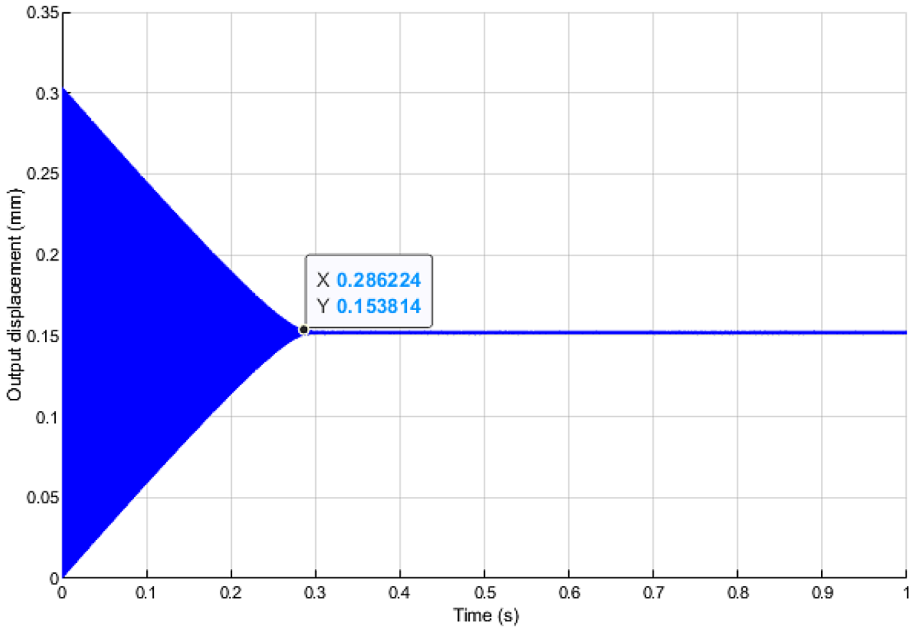

Figure 5. Matlab Simulink simulations (without oil damping)

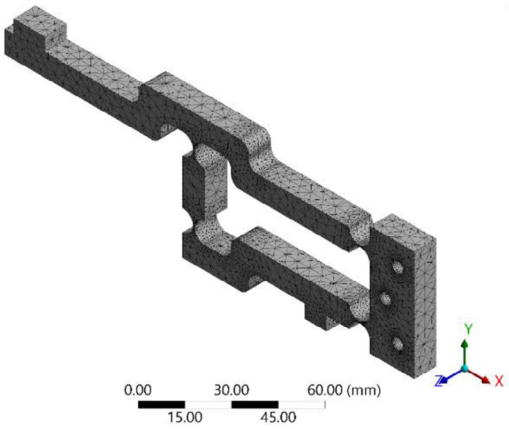

(a) Model meshing

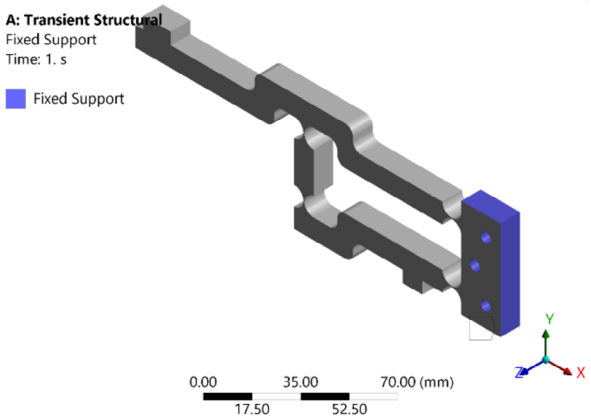

(b) Modl boundary conditions

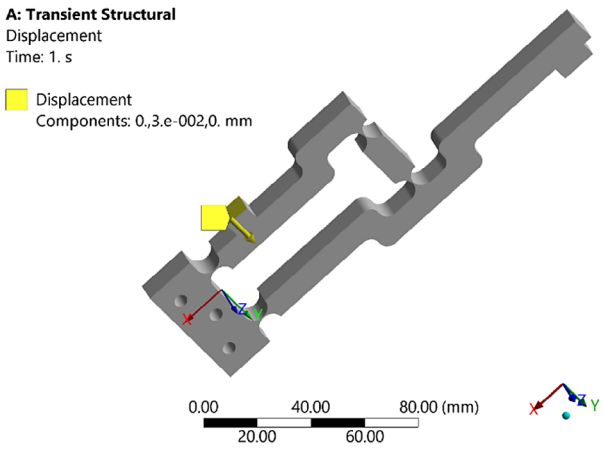

(c) Displacement input

Figure 6. Ansys model

shown in Figure 6, and the PZT generates an input displacement of 0.03 mm.

From Figure 7, it can be observed that with the input displacement of the mechanism x_i = 0.03 mm, the output displacement x_o = 0.15 mm corresponds to the amplification ratio of the mechanism A_{amp} = 5. The maximum Von Mises stress on the mechanism structure is σ_{max} = 237.05 MPa that satisfies constraint relating to the strength of material.

The transient response simulation of the flexure mechanism results show the time-response of the output displacement of the flexure mechanism are expressed in Figure 8 or 9, respectively with or without considering viscous damping. In Figure 9, it is shown that the response time and overshoot of the mechanism using viscous damping are significantly smaller than those without using viscous damping. The response time with viscous damping

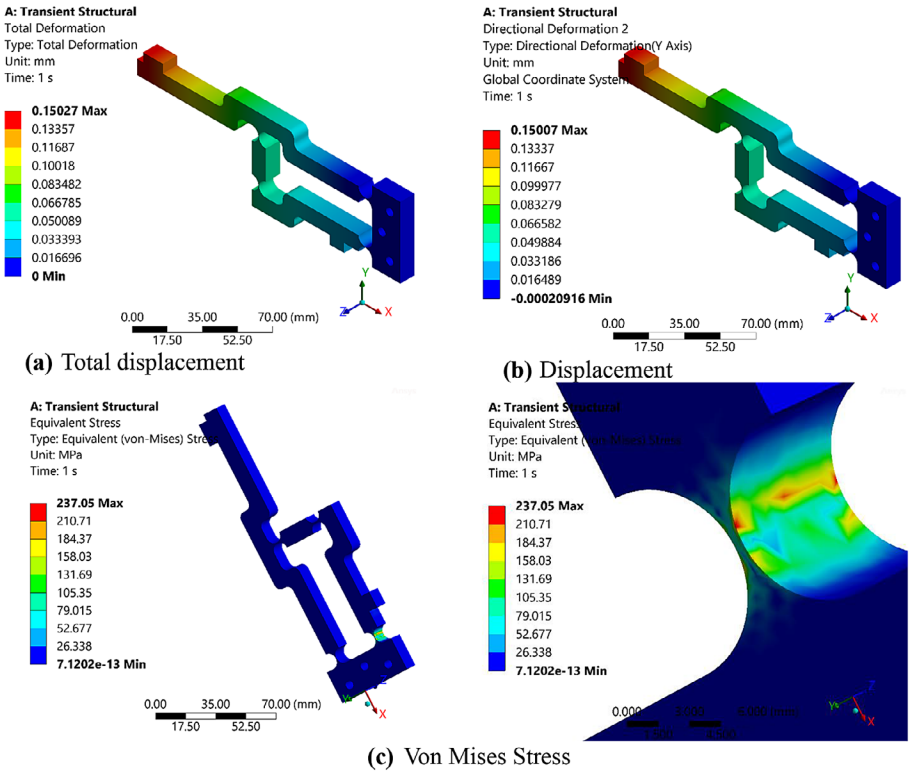

Figure 7. Simulation results — (a) total displacement, (b) displacement, (c) von mises stress

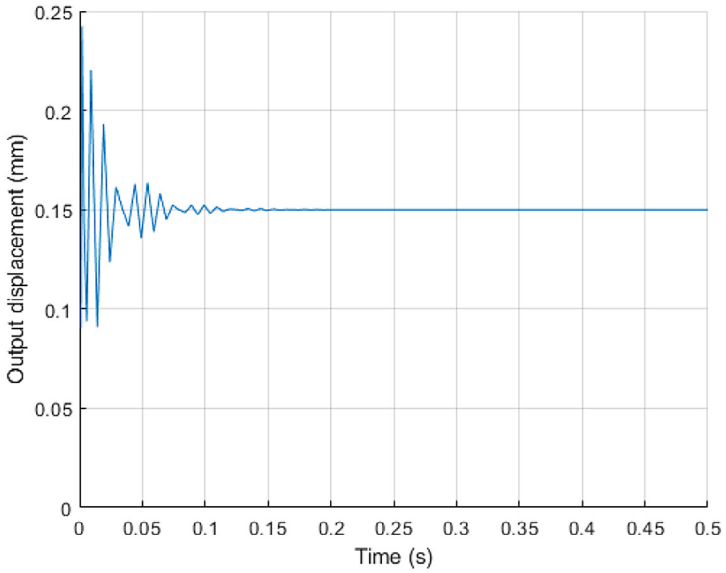

Figure 8. ANSYS simulation results – without viscous damping

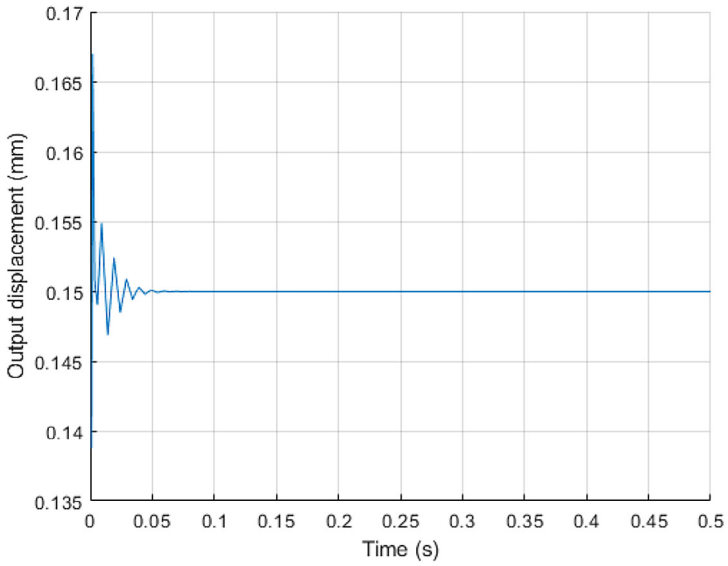

Figure 9. ANSYS simulation results – with viscous damping

is approximately 0.05 s, while the one without viscous damping is greater, approximately 0.1 s. The results also show that the overshoot is much smaller and better when simulating with considering viscous damping of lubrication oil. From the simulation, with an input displacement of 0.03 mm, the overshoot of the output can be seen as 0.1 mm and the 0.018 mm respectively corresponding to without and with viscous damping. We can see the difference between Matlab and Ansys models because of idealizing assumptions about structure mechanics in pseudo rigid body model.

EXPERIMENTS

To validate the mathematical and simulation models (Matlab Simulink and Ansys models), experiments were conducted to perform the dynamic analysis. The designed mechanism was made of carbon steel C45 and fabricated by EDM wire-cutting based on dimensions in Table 1. The flexure mechanism was used to perform the experiment shown in Figure 10.

An experimental setup was arranged as shown in Figure 11 to evaluate the effect of viscous damping on the transient response of the flexure mechanism under the open-loop displacement control. MDT694A PZT actuator controller (THORLABS) generates, amplifies and provides the input voltage to the PZT actuator. A non-contact laser displacement sensor LK-G30 (Keyence) is used to measure the output displacement of the mechanism with an accuracy of 0.01 μm and a measurement range of ±5 mm. A micro-positioning stage was used to adjust the focal point for the laser sensor. All devices were mounted on an anti-vibration table to isolate external vibrations

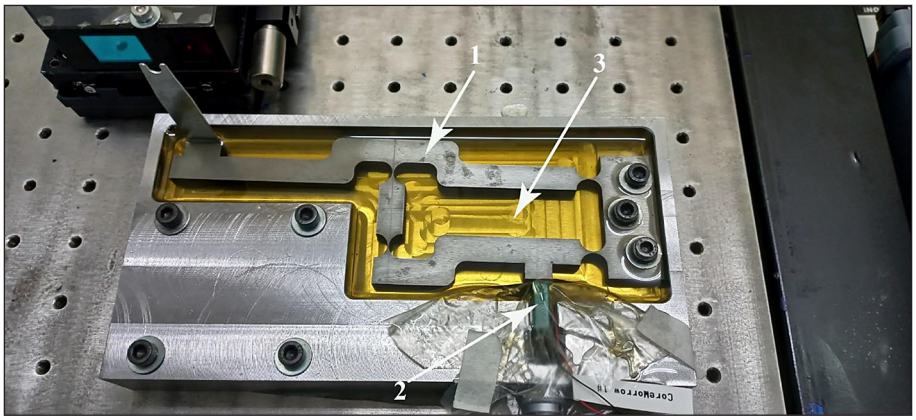

Figure 10. Flexure mechanism dipped to lubrication oil. (1) flexure mechanism; (2) PZT actuator; (3) lubrication oil

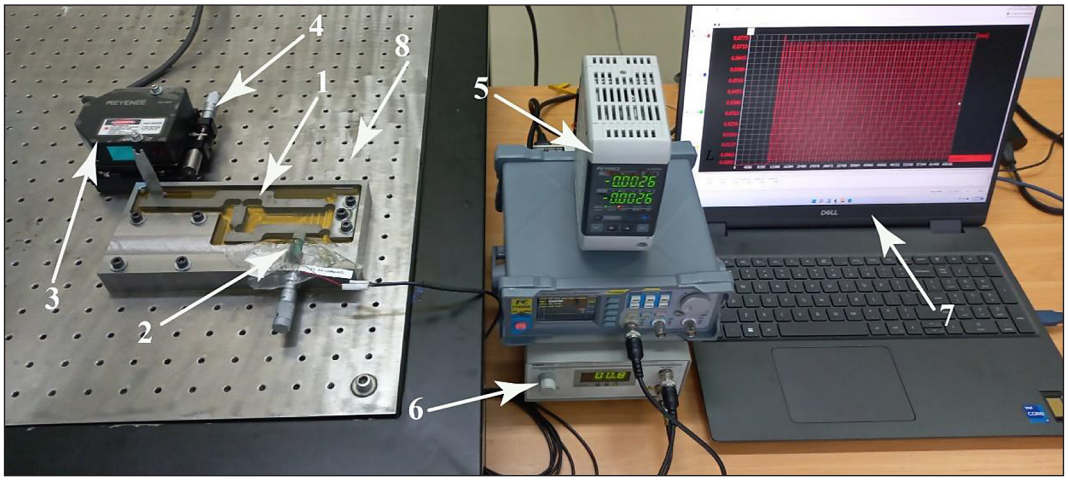

Figure 11. Full set of experiment devices. (1) flexure mechanism; (2) PZT actuator; (3) laser displacement sensor LK – G30; (4) micro-positioning stage; (5) sensor controller LK – 3001P; (6) PZT driver MDT694A; (7) laptop for controlling; (8) vibration isolation table

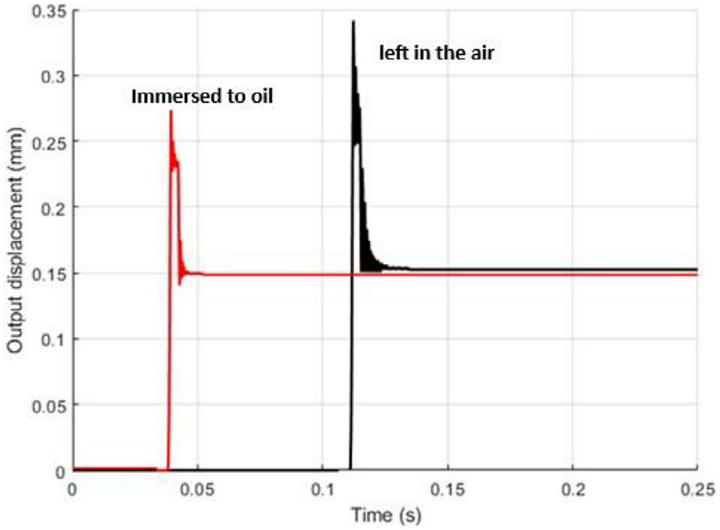

(a) - zoom out

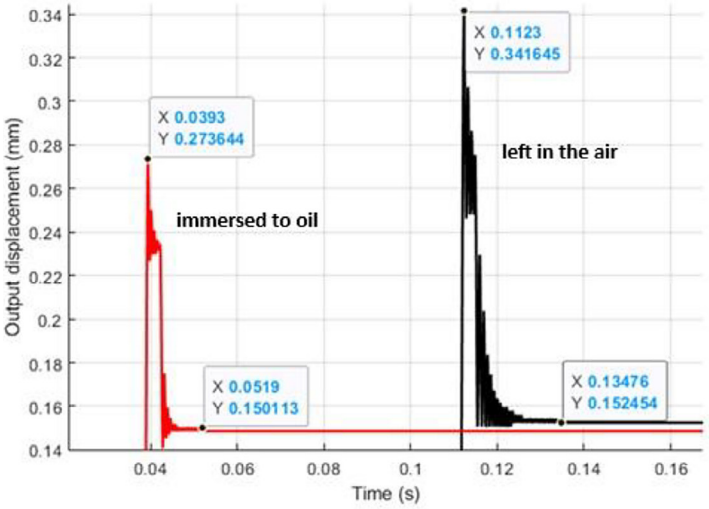

(b) – zoom in

Figure 12. Experimental results with or without viscous damping (immersed to oil or left in the air)

from affecting measurement accuracy. The measurement data was transmitted through the LK-3001P controller to the computer via USB. The data was displayed using LK-Navigator software (Keyence). The measured displacement results are shown in Figure 12 which shows the transient response of the output displacement of the compliant mechanism with open-loop control in two cases: immersed to oil and left in the air. The output displacement results show that the response times of the mechanism with or without lubrication oil are respectively at 0.05 s and 0.1 s. Figure 12 also shows that the overshoot of the mechanism in the lubrication oil condition is 0.272 mm, in comparison with 0.341 mm, the one without lubrication oil. These experimental results show that both the overshoot and response time are better in the presence of lubrication oil.

The experiment proved that the mathematic and Matlab Simulink model and Ansys model are effective to study the dynamic analysis of flexure mechanism with considering viscous damping of the working environment. The study leads to the transient response of flexure mechanism will be improved when working dipped to lubrication oil – with viscous damping: 0.05 s, 0.272 mm; and without viscous damping: 0.1 s, 0.341 mm.

CONCLUSIONS

This study proposes a new approach: dynamic analysis of flexure-based mechanisms operating in non-air environments such as lubrication oil. The mechanism was designed and analytically modeled when counting the viscous damping of lubrication oil. Then the mathematical model is simulated using Matlab Simulink. Ansys simulation considering viscous damping effect was conducted to show the dynamic response of the finite element model. The flexure mechanism was manufactured using wire-cutting CNC machine, the mechanism is used to perform experiments with a Thorlabs PZT actuator and a Keyence laser displacement sensor to observe the dynamic response of the flexure mechanism in both cases dipped to the oil and left in the air. Results received from modeling and simulations using Matlab Simulink, Ansys, and also results obtained from experiments show that the overshoot, response time and stress inside the structure significantly reduce when changing the working environment from "left in the air" to "immersed in lubrication oil". These findings validate the effectiveness of viscous damping and suggest potential of its application for future closed-loop control implementation. This brings us a new study direction about realized applications of flexure mechanisms concerning their working environment such as the immersion of flexure system into oil to get a faster stabilization of flexure stages, to reduce wear and prevent corrosion, and ensure long-term reliability, and to reduce drift and vibration.

Acknowledgments

This work was financially supported by Ho Chi Minh City University of Industry and Trade under Contract no 05/HĐ-DCT dated 09 Jan 2024.

REFERENCES

1. Nguyen V-K, Pham H-T, Pham H-H, Dang Q-K. Optimization design of a compliant linear guide for high-precision feed drive mechanisms. Mechanism and Machine Theory. 2021;165:104442. https://doi.org/10.1016/j.mechmachtheory.2021.104442
2. Li H, Tang H, Li J, Chen X. Design, fabrication, and testing of a 3-DOF piezo fast tool servo for microstructure machining. Precision Engineering. 2021;72:756–68. https://doi.org/10.1016/j.precisioneng.2021.07.015
3. Song T, Pan M, Ling M, Wu S, Chen T. Design and modeling of a piezoelectric stick-slip actuator with an asymmetric rhombus-type compliant mechanism. Smart Materials and Structures. 2025. https://doi.org/10.1088/1361-665X/adefa5
4. Phan T-V, Truong VM, Pham H-T, Nguyen V-K. Design of a novel large-stroke compliant constant-torque mechanism based on chained beam-constraint model. Journal of Mechanisms and Robotics. 2024;16(8):081006. https://doi.org/10.1115/1.4063980
5. Chen W, Fan Z, Lu Q, Xu Y, Li Z, Wei H, et al. Nonlinear design, analysis, and testing of a single-stage compliant orthogonal displacement amplifier with a single input force for micro-grippers. Journal of Micromechanics and Microengineering. 2024;34(7):075010. https://doi.org/10.1088/1361-6439/ad5a19
6. Lyu Z, Xu Q. A compliant constant-force mechanism with sub-Newton force and millimeter stroke output. Sensors and Actuators A: Physical. 2024;374:115465. https://doi.org/10.1016/j.sna.2024.115465
7. Ding B, Zhao J, Li Y. Design of a spatial constant-force end-effector for polishing/deburring operations. The International Journal of Advanced

Manufacturing Technology. 2021;116(11):3507–15. https://doi.org/10.1007/s00170-021-07579-1

8. Zhang J, Zhao L, Li L, Ma F, Chen G. Design of passive constant-force end-effector for robotic polishing of optical reflective mirrors. Chinese Journal of Mechanical Engineering. 2022;35(1):141. https://doi.org/10.1186/s10033-022-00811-3
9. Ling M, He X, Wu M, Cao L. Dynamic design of a novel high-speed piezoelectric flow control valve based on compliant mechanism. IEEE/ASME Transactions on Mechatronics. 2022;27(6):4942–50. https://doi.org/10.1109/TMECH.2022.3169761
10. Zhang Y, Zhang X, Xie D, Cao S, Yang B. Mechanism and validation of a long-stroke ultraprecision atmospheric pressure driven actuator. IEEE/ASME Transactions on Mechatronics. 2024;29(5):3750–61. https://doi.org/10.1109/TMECH.2024.3359179
11. Lobontiu N. Compliant mechanisms: design of flexure hinges: CRC press; 2002.
12. Howell LL, Magleby SP, Olsen BM, Wiley J. Handbook of compliant mechanisms: Wiley Online Library; 2013.
13. Wu H, Zhang Y, Li L, Bai R, Wang H, Chen G. Design and control of a lever-bridge differential displacement reducer with sub-nanometer resolution. IEEE Transactions on Automation Science and Engineering. 2025. https://doi.org/10.1109/TASE.2025.3572151
14. Gui S, Zhang S, Fu B, Ling M. Fluid-dynamic analysis and multi-objective design optimization of piezoelectric servo valves. Flow Measurement and Instrumentation. 2022;85:102157. https://doi.org/10.1016/j.flowmeasinst.2022.102157
15. Zhao D, Zhu B, Du H, Shi Z, Zhu Z. Topology optimization of a dual-axial piezo-actuated fast tool servo with decoupled kinematics. Precision Engineering. 2025. https://doi.org/10.1016/j.precisioneng.2025.04.023
16. Chen W, Kang S, Lu Q, Zhang Q, Wei H, Zhang Y, et al. A novel bridge-type compliant displacement amplification mechanism under compound loads based on the topology optimisation of flexure hinge and its application in micro-force sensing. Smart Materials and Structures. 2023;33(1):015020. https://doi.org/10.1088/1361-665X/ad1316
17. Ling M, Cao J, Jiang Z, Zeng M, Li Q. Optimal design of a piezo-actuated 2-DOF millimeter-range monolithic flexure mechanism with a pseudo-static model. Mechanical Systems and Signal Processing. 2019;115:120-31. https://doi.org/10.1016/j.ymssp.2018.05.064
18. Chen Z, Shi J, Wang K, Zhang X. Damped two-axis axially collocated flexure hinge. Review of Scientific Instruments. 2023;94(6). https://doi.org/10.1063/5.0149319
19. Guo F, Sun Z, Zhang S, Cao R, Li H. Dynamic characteristics and frequency reliability analysis of an optimized compliant stroke amplification mechanism. Journal of Mechanisms and Robotics. 2023;15(6):061007. https://doi.org/10.1115/1.4056376
20. Chun H, Kim GH, Villarraga-Gómez H, Kim H-Y, Elwany A, Lee C. Characterization of thermally stable compliant structures with internal fluidic channels. Precision Engineering. 2020;66:201-8. https://doi.org/10.1016/j.precisioneng.2020.07.013
21. Paros JM. How to design exural hinges. Mach Design. 1965;37:151–6.